High-spin spectroscopy of ^{122}I

Purnima Singh, Somnath Nag, K. Selvakumar, and A. K. Singh
Department of Physics & Meteorology, Indian Institute of Technology Kharagpur, IN-721302, India

I. Ragnarsson
Division of Mathematical Physics, LTH, Lund University, Box 118, S-22100 Lund, Sweden

Abhijit Bisoi and A. Goswami
Nuclear Physics Division, Saha Institute of Nuclear Physics, Kolkata, 700064, India

S. Bhattacharya
Applied Nuclear Physics Division, Saha Institute of Nuclear Physics, Kolkata, 700064, India

S. Kumar and K. Singh
Department of Physics, Punjab University, Chandigarh, 160014, India

J. Sethi, Sudipta Saha, T. Trivedi, S. V. Jadhav, R. Donthi, B. S. Naidu, and R. Palit
Deptartment of Nuclear and Atomic Physics, Tata Institute of Fundamental Research, Mumbai, 400005, India
(Received 2 March 2012; published 15 May 2012)

High-spin states in ^{122}I have been investigated using the ^{116}Cd(^{11}B,5n)^{122}I reaction at a beam energy of 65 MeV and γ-ray coincidence events were recorded with the INGA spectrometer. The level scheme of ^{122}I has been extended up to spin $I = 30$. Experimental features, such as band-crossing frequencies, aligned angular momenta, signature splitting, and $B(M1)/B(E2)$ ratios have been used for configuration assignments to low-energy band structures. Maximally aligned states involving all eight particles outside the ^{114}Sn core and states with one particle antialigned have been identified. Cranked Nilsson-Strutinsky calculations have been used to interpret high-spin structures.

DOI: 10.1103/PhysRevC.85.054311 PACS number(s): 21.10.−k, 23.20.Lv, 23.20.En, 27.60.+j

I. INTRODUCTION

The iodine ($Z = 53$) nuclei lie between the spherical ($Z = 50$) and the well-deformed ($Z = 58$) region and are of considerable interest because of competing shape driving tendencies of the orbitals occupied by the neutrons and the protons. The orbitals available near the Fermi surface of these nuclei are $h_{11/2}$, $g_{9/2}$, $g_{7/2}$, and $d_{5/2}$ for protons and $h_{11/2}$, $g_{7/2}$, $d_{5/2}$, and $d_{3/2}$ for neutrons. Spectroscopic investigations carried out in the odd-A $^{113–125}$I nuclei have revealed several bands based upon $\pi g_{7/2}(d_{5/2})$ and $\pi h_{11/2}$ orbitals. These bands are associated with moderately deformed prolate and oblate shapes. In addition, bands based upon particle-hole excitations involving $\pi g_{9/2}$ extruder orbitals, which play a decisive role in the development of collective bands in Sn and Sb nuclei, also persist in the iodine nuclei. High-spin structures in these nuclei are described by abrupt appearance of energetically favored noncollective oblate states and coexistence of weakly collective and noncollective quasiparticle-aligned configurations [1–10].

Recent spectroscopic studies of ^{123,125}I nuclei revealed maximally aligned states involving all the particles outside the ^{114}Sn core [5,6]. In addition to these states, noncollective states with the angular momentum of one and two particles antialigned with respect to the rotation axis were also identified in these nuclei. Since a maximally aligned state is formed by exhausting all the spin available within the valence space, further angular momentum can only be generated by particle-hole excitations from the core. In ^{123}I, a large number of weak, high-energy transitions were observed feeding the maximally aligned states [5]. These transitions were proposed to originate from states based on configurations involving a core-breaking neutron particle-hole excitation from the $g_{7/2}(d_{5/2})$ to the $d_{3/2}s_{1/2}$ or $h_{11/2}$ orbitals across the semimagic $N = 64$ shell gap. Similar features were also reported in ^{121}I [10].

Therefore, in view of the wide variety of structural features observed in the odd-A iodine nuclei, it is of interest to probe analogous features in odd-odd I nuclei. However, information available about the high-spin structures in heavier ($A > 120$) odd-odd I nuclei are limited.

In the present work we document the results of an in-beam study of the high-spin states in ^{122}I obtained with the Indian National Gamma-ray Array (INGA) spectrometer. The previously known level scheme [11,12] is extended considerably. Maximally aligned valence-space configurations and states with one particle antialigned have been observed. Weakly collective bands based on configurations involving particle-hole excitations from the ^{114}Sn core have been observed to feed the maximally aligned noncollective levels.

In Sec. II the experimental setup and the off-line data analysis technique are briefly discussed. The experimental results and the ^{122}I level scheme are presented in Sec. III. The results are discussed within the framework of the cranked Nilsson-Strutinsky (CNS) model and cranked shell model (CSM) in Sec IV. Finally, a brief summary of the present work is given in Sec. V.

II. EXPERIMENTAL DETAILS AND DATA ANALYSIS

High spin states of ^{122}I were studied using heavy-ion fusion evaporation reaction ^{116}Cd(^{11}B,5n)^{122}I. The ^{11}B beam with an energy of 65 MeV and intensity 1.5 nA was provided by the 14 UD TIFR-BARC pelletron accelerator at TIFR, Mumbai. The target consisted of enriched ^{116}Cd of thickness 15 mg/cm^2. The γ-ray coincidence events were measured with the INGA spectrometer consisting of 15 Compton-suppressed clover detectors arranged in six rings [13,14]. In a beam time of 3 days, a total of 3.1×10^9 coincidence events with fold $\geqslant$2 were collected.

For the off-line analysis, the calibrated and gain-matched data were sorted into γ-γ matrices and γ-γ-γ cubes. The software package RADWARE [15] was used for the data analysis. To determine multipolarity of γ-ray transitions, the coincidence events were sorted into two angular distribution matrices. One matrix contained events detected at an angle of 23° (23) on one axis and all events (all) on the other axis. The second matrix contained events detected at 90° (90) on one axis and all events on the other axis. Gates were set in these matrices on the axis with events detected in all detectors. The angular distribution ratio

$$R_\theta = \frac{I(\gamma 2_{23}, \gamma 1_{\rm all})}{I(\gamma 2_{90}, \gamma 1_{\rm all})}$$

are 1.4 and 0.65 for stretched quadrupole and dipole transitions, respectively. The values were determined from transitions of known multipolarity in ^{123}I [16], which was one of the dominant channels in the present experiment.

Multipolarity assignments were further corroborated by extracting γ-ray linear polarizations in order to distinguish between electric (EL) and magnetic (ML) character. This can be achieved by considering the four crystals within a single clover detector of the INGA spectrometer as Compton polarimeters, where individual crystals act as scatterer, and the two adjacent crystals as observer [17,18]. For coincidence polarization measurements the integrated polarization-directional correlation from oriented nuclei (IPDCO) procedure was applied [17,18]. Two asymmetric matrices were constructed from the coincidence data corresponding to single hits in any detector on one axis against clover double-hit scattering events of 90° detector on the second axis. The scattering events are defined as either perpendicular to the reaction plane (first matrix) or parallel to the reaction plane (second matrix). The number of perpendicular $N_\perp$ and parallel $N_\parallel$ scatters for a given γ ray were obtained by projecting out spectra gated by specific ^{122}I transitions on the single-hit axis of the respective matrix. Assuming that all the clover crystals have equal efficiencies, the experimental polarization asymmetry parameter was calculated as

$$\Delta_{\rm asym} = \frac{a(E_\gamma)N_\perp - N_\parallel}{a(E_\gamma)N_\perp + N_\parallel},$$

where $a(E_\gamma)$ is a scaling factor which corresponds to the ratio of the horizontal versus vertical coincidence count rates measured without polarization. It is a function of γ-ray energy. A positive asymmetry value is expected for electric transitions, while a negative difference is expected for magnetic transitions. A near-zero value is indicative of a possible admixture. The validity of the method of IPDCO measurement was verified from the known transitions in ^{123}I [16] (see Fig. 1).

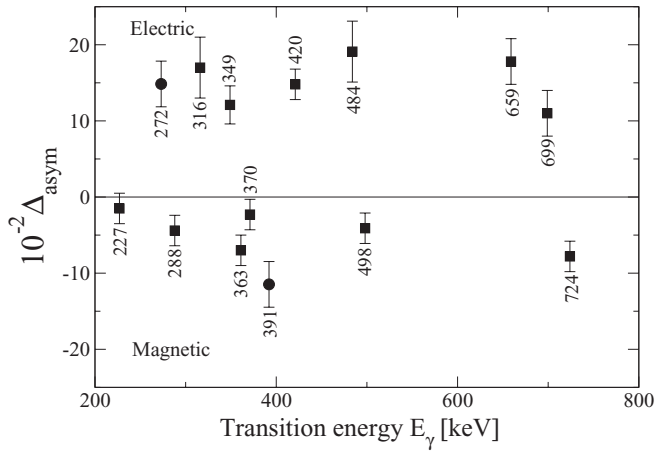

FIG. 1. Experimental γ-ray asymmetry parameter $\Delta_{\rm asym}$ from polarization measurements plotted for transitions of ^{122}I (closed square). Known transitions of ^{123}I (closed circle) [16] are also included for reference.

III. RESULTS AND LEVEL SCHEME

The level scheme of ^{122}I is shown in Fig. 2. Spins and parities of the levels have been assigned with the help of angular distribution ratios and IPDCO measurements. In some cases, the presence of crossover and interband transitions helped in assigning spins. The γ-ray energies, intensities, angular distribution ratios, adopted multipolarities, level energies, and spin assignment for all the observed transitions in ^{122}I are listed in Table I.

A. Low-spin results

Low-lying states in ^{122}I were studied from the radioactive decay of ^{122}Xe, and the spin and parity of the ground state had been assigned as $I^\pi = 1^+$ with a half-life of 3.63 m [19]. Later, several experiments were performed to study its high-spin states [12,20,21], however, there were ambiguities in spin-parity assignments to the band structures. Recently, Moon *et al.* has reported several isomeric states with firm excitation energies in ^{122}I. In this work we have adopted the low-lying level structure up to $I^\pi = 8^-$ state from the previous work [22].

Bands labeled 1–12 were reported by Moon *et al.* [11,12,19,22]. In the present work we confirm most of the previous results and observe certain new results which are summarized in the following. A new level with $I^\pi = 17^-$ has been added to band 3 with two decay-out transitions of energies 1050.0 and 592.2 keV. Several dipole transitions of energies 380.4, 506.6, 662.7, 298.9, and 439.1 keV, linking bands 5 and 6, have been observed in the present work. We could also extend the bands 7 and 8 with the help of γ rays of energies 836.8 and 786.2 keV,

TABLE I. Energies, intensities, angular distribution ratios, adopted multipolarities, level energies, and spin assignments of γ-ray transitions of ^{122}I.

Energy E_γ [a] (keV)	Intensity I_γ [b]	Intensity Ratio R_θ	Multipolarity Assignment	Initial Level Energy E_i (keV)	Spin Assignment $J_i^\pi \rightarrow J_f^\pi$
148.2	181(10)	0.87(10)	$E1$	1 166	$10^+ \rightarrow 9^-$
184.0	431(23)	0.83(7)	$M1$	3 009	$16^+ \rightarrow 15^+$
226.7[c]	552(25)	0.67(5)	$M1$	746	$9^- \rightarrow 8^-$
237.7			$M1$	2 013	$11^- \rightarrow 10^-$
241.1	100(4)	0.72(7)	$M1$	5 462	$21^- \rightarrow 20^-$
245.6			$M1$	1 490	$11^- \rightarrow 10^-$
248.8	3(1)			10 834	$\rightarrow 30$
266.7			$M1$	5 221	$20^- \rightarrow 19^-$
267.9	43(3)		$M1$	4 218	$18^+ \rightarrow 17^+$
273.4		0.85(14)	$M1$	718	$9^- \rightarrow 8^-$
287.6[c]	621(30)	0.62(5)	$M1$	746	$9^- \rightarrow 8^-$
289.0	127(9)	0.43(4)	$M1$	1 825	$12^+ \rightarrow 11^+$
298.9[d]			$M1$	3 642	$16^- \rightarrow 15^-$
300.5	384(18)	0.58(5)	$M1$	2 825	$15^+ \rightarrow 14^+$
307.6	120(7)		$M1$	2 988	$14^- \rightarrow 14^-$
312.2			$M1$	4 518	$18^- \rightarrow 17^-$
315.6[d]			$M1$	2 650	$13^- \rightarrow 12^-$
316.3[c]	69(4)	0.68(7)	$E1$	5 462	$21^- \rightarrow 20^+$
321.2	106(7)		$M1$	2 334	$12^- \rightarrow 11^-$
324.0	64(5)		$M1$	2 681	$14^- \rightarrow 13^-$
338.5	38(4)	0.54	$M1$	2 988	$14^- \rightarrow 13^-$
339.6	167(10)	0.54(7)	$M1$	2 525	$14^+ \rightarrow 13^+$
349.4[c]	234 (12)	1.41(11)	$E2$	5 495	$22^+ \rightarrow 20^+$
350.7	0.70(10)		$M1$	1 068	$10^- \rightarrow 9^-$
351.0	80(5)		$M1$	2 072	$12^- \rightarrow 11^-$
351.3[d]			$M1$	3 951	$17^+ \rightarrow 16^+$
359.7	431(23)	0.46(6)	$M1$	2 185	$13^+ \rightarrow 12^+$
360.3	153(7)		$M1$	1 850	$12^- \rightarrow 11^-$
362.9[c]	274(12)	0.55(3)	$M1$	1 109	$10^- \rightarrow 9^-$
363.7	28(3)		$M1$	1 623	$11^- \rightarrow 10^-$
367.7	46(4)		$M1$	3 774	$16^- \rightarrow 15^-$
370.1[c]	278(15)	0.40(4)	$M1$	1 536	$11^+ \rightarrow 10^+$
375.9	129(6)		$M1$	1 444	$11^- \rightarrow 10^-$
380.3	1280(65)	1.48(9)	$E2$	1 166	$10^+ \rightarrow 8^+$
380.4	78(4)		$M1$	1 490	$11^- \rightarrow 10^-$
388.7	18(3)	0.57(5)	$M1$	8 593	$27^- \rightarrow 26^-$
397.2	83(6)		$M1$	1 841	$12^- \rightarrow 11^-$
405.9	65(4)		$M1$	1 850	$12^- \rightarrow 11^-$
418.4	61(4)		$M1$	3 407	$15^- \rightarrow 14^-$
419.8[c]	400(20)	0.67(5)	$E1$	1 166	$10^+ \rightarrow 9^-$
427.1	65(3)	1.33(7)	$E2$	5 462	$21^- \rightarrow 19^-$
431.3	35(3)		$M1$	2 503	$13^- \rightarrow 12^-$
431.5			$M1$	4 206	$17^- \rightarrow 16^-$
431.7	31(3)		$M1$	2 273	$13^- \rightarrow 12^-$
436.2			$M1$	4 954	$19^- \rightarrow 18^-$
439.1	3(1)		$M1$	4 606	$18^- \rightarrow 17^-$
443.4			$M1$	2 067	$12^- \rightarrow 11^-$
456.4	24(2)		$M1$	2 730	$14^- \rightarrow 13^-$
457.8[d]			$M1$	3 674	$16^- \rightarrow 15^-$
476.8	31(2)		$M1$	1 721	$11^- \rightarrow 10^-$
478.7			$M1$	2 545	$13^- \rightarrow 12^-$
484.5[c]	122(8)	1.20(6)	$E2$	3 009	$16^+ \rightarrow 14^+$
485.0[c]			$M1$	2 988	$14^- \rightarrow 13^-$
486.5			$M1$	3 216	$15^- \rightarrow 14^-$
497.7c	65(4)	0.50(3)	$M1$	1 244	$10^- \rightarrow 9^-$

TABLE I. (*Continued.*)

Energy E_γ [a] (keV)	Intensity I_γ [b]	Intensity Ratio R_θ	Multipolarity Assignment	Initial Level Energy E_i (keV)	Spin Assignment $J_i^\pi \rightarrow J_f^\pi$
498.3	68(5)	0.40(3)	$M1$	1 018	$9^- \rightarrow 8^-$
505.3			$M1$	3 051	$14^- \rightarrow 13^-$
506.6			$M1$	2 357	$13^- \rightarrow 12^-$
529.9	15(2)	1.38(8)	$E2$	9 123	$29^- \rightarrow 27^-$
541.9	42(3)		$M1$	1 260	$10^- \rightarrow 9^-$
544.2			$M1$	3 048	$14^- \rightarrow 13^-$
548.2	41(3)	0.53(4)	$M1$	6 010	$22^- \rightarrow 21^-$
554.9			$M1$	1 623	$11^- \rightarrow 10^-$
558.9	403(18)	1.37(10)	$E2$	2 334	$12^- \rightarrow 10^-$
559.2			$M1$	1 018	$9^- \rightarrow 8^-$
566.2			$M1$	1 775	$10^- \rightarrow 9^-$
589.1	12(2)		$M1$	7 203	$24^- \rightarrow 23^-$
592.2			$M1$	4 266	$17^- \rightarrow 16^-$
603.4	45(4)	0.70(6)	$M1$	6 614	$23^- \rightarrow 22^-$
611.6	73(4)		$M1$	1 721	$11^- \rightarrow 10^-$
619.2	32(4)		$E2$	4 218	$18^+ \rightarrow 16^+$
624.1			$E2$	1 068	$10^- \rightarrow 8^-$
629.9	14(2)			7 244	$\rightarrow 23^-$
636.8			$E2$	2 650	$13^- \rightarrow 11^-$
640.1	279(15)	1.20(4)	$E2$	2 825	$15^+ \rightarrow 13^+$
640.6	94(7)	0.59(5)	$M1$	3 650	$17^+ \rightarrow 16^+$
648.7	175(9)	1.35(12)	$E2$	2 185	$13^+ \rightarrow 11^+$
650.5	268(13)		$E2$	1 109	$10^- \rightarrow 8^-$
652.7	85(4)		$M1$	1 721	$11^- \rightarrow 10^-$
654.1	392(21)	1.33(10)	$E2$	2 988	$14^- \rightarrow 12^-$
659.1[c]	1000	1.35(6)	$E2$	1 825	$12^+ \rightarrow 10^+$
662.7			$M1$	3 343	$15^- \rightarrow 14^-$
665.9			$M1$	1 775	$10^- \rightarrow 10^-$
683.6	8(1)	0.61(6)	$M1$	7 886	$25^- \rightarrow 24^-$
689.3			$M1$	1 209	$9^- \rightarrow 8^-$
699.3[c]	635(32)	1.34(7)	$E2$	2 525	$14^+ \rightarrow 12^+$
702.9	185(9)	1.41(12)	$E2$	5 221	$20^- \rightarrow 18^-$
702.9	187(10)		$E2$	1 721	$11^- \rightarrow 9^-$
706.7	6(1)		$E2$	8 593	$27^- \rightarrow 25^-$
706.8	4(1)			8 984	
724.1[d]	143(7)	0.50(4)	$M1$	6 219	$23^+ \rightarrow 22^+$
724.4	209(10)	1.21(7)	$E2$	1 244	$10^- \rightarrow 8^-$
726.6	107(7)		$E2$	1 444	$11^- \rightarrow 9^-$
732.0	28(2)		$E2$	1 841	$12^- \rightarrow 10^-$
740.7	165(9)	1.44(12)	$E2$	1 850	$12^- \rightarrow 10^-$
743.3	290(15)	1.42(14)	$E2$	1 490	$11^- \rightarrow 9^-$
743.7	326(13)	1.35(10)	$E2$	4 518	$18^- \rightarrow 16^-$
748.4			$E2$	4 954	$19^- \rightarrow 17^-$
753.6	3(1)			11 108	$\rightarrow 30$
756.9	200(9)		$E2$	3 407	$15^- \rightarrow 13^-$
757.2			$M1$	1 775	$10^- \rightarrow 9^-$
773.1	48(3)		$E2$	1 841	$12^- \rightarrow 10^-$
781.8	52(3)		$E2$	1 850	$12^- \rightarrow 10^-$
782.3	185(10)		$E2$	2 503	$13^- \rightarrow 11^-$
786.1	396(19)	1.40(11)	$E2$	3 774	$16^- \rightarrow 14^-$
786.2	40(3)		$E2$	5 035	$19^- \rightarrow 17^-$
788.1	146(8)	1.23(8)	$E2$	4 249	$17^- \rightarrow 15^-$
789.3	92(4)	1.41(10)	$E2$	6 010	$22^- \rightarrow 20^-$
797.8	13(1)		$E1$	2 334	$12^- \rightarrow 11^+$
799.2	189(13)		$E2$	4 206	$17^- \rightarrow 15^-$
803.2	14(2)		$E1$	2 988	$14^- \rightarrow 13^+$
803.9[d]			$E2$	2 013	$11^- \rightarrow 9^-$

TABLE I. (*Continued*.)

Energy E_γ [a] (keV)	Intensity I_γ [b]	Intensity Ratio R_θ	Multipolarity Assignment	Initial Level Energy E_i (keV)	Spin Assignment $J_i^\pi \rightarrow J_f^\pi$
805.9	99(6)	1.12(10)	$E2$	7 025	$25^+ \rightarrow 23^+$
807.1			$E2$	2 067	$12^- \rightarrow 10^-$
815.3	35(3)	1.46(23)	$E2$	1 260	$10^- \rightarrow 8^-$
823.9	35(3)	1.19(5)	$E2$	4 167	$17^- \rightarrow 15^-$
827.8	105(7)	1.39(9)	$E2$	2 072	$12^- \rightarrow 10^-$
828.9	78(5)	1.57(14)	$E2$	2 273	$13^- \rightarrow 11^-$
830.6	83(6)	1.48(9)	$E2$	2 681	$14^- \rightarrow 12^-$
836.8	25(4)	1.25(6)	$E2$	3 884	$16^- \rightarrow 14^-$
839.3	79(6)		$E2$	2 681	$14^- \rightarrow 12^-$
866.9	223(12)	1.27(4)	$E2$	2 357	$13^- \rightarrow 11^-$
888.1	39(4)		$E2$	2 730	$14^- \rightarrow 12^-$
922.1			$E2$	2 545	$13^- \rightarrow 11^-$
927.3	267(13)	1.36(6)	$E2$	5 146	$20^+ \rightarrow 18^+$
941.4	56(4)		$M1$	3 951	$17^+ \rightarrow 16^+$
942.9	18(2)	1.20(7)	$E2$	3 216	$15^- \rightarrow 13^-$
944.3			$E2$	3 674	$16^- \rightarrow 14^-$
949.2	12(2)		$E1$	3 774	$16^- \rightarrow 15^+$
957.4	93(6)	1.24(6)	$E2$	3 461	$15^- \rightarrow 13^-$
961.3	11(1)	0.55(6)	$M1$	4 611	$18^+ \rightarrow 17^+$
961.6	60(5)	1.40(10)	$E2$	3 642	$16^- \rightarrow 14^-$
964.1[d]			$E2$	4 606	$18^- \rightarrow 16^-$
975.5	67(4)	1.29(8)	$E2$	3 048	$14^- \rightarrow 12^-$
984.0			$E2$	3 051	$14^- \rightarrow 12^-$
986.7	104(7)	1.29(8)	$E2$	3 343	$15^- \rightarrow 13^-$
989.3			$M2$	1 775	$10^- \rightarrow 8^+$
1001.6	25(4)	1.28(10)	$E2$	8 204	$26^- \rightarrow 24^-$
1039.7	30(3)	1.11(8)	$E2$	4 639	$18^+ \rightarrow 16^+$
1050.0			$E2$	4 266	$17^- \rightarrow 15^-$
1070.2	4(1)			9 395	$\rightarrow 27^+$
1074.6	71(5)	1.20(9)	$E2$	3 599	$16^+ \rightarrow 14^+$
1099.9	13(1)	1.60(24)	$E2$	9 425	$29^+ \rightarrow 27^+$
1117.1	5(1)	0.51(10)	$M1$ or $E1$	10 240	$30 \rightarrow 29^-$
1125.4	50(3)		$E2$	3 951	$17^+ \rightarrow 15^+$
1125.6[d]	25(3)			4 775	$\rightarrow 17^+$
1160.2	4(1)		$M1$ or $E1$	10 585	$30 \rightarrow 29^+$
1169.1	14(2)	0.42(5)	$M1$ or $E1$	8 194	$26 \rightarrow 25^+$
1192.5	35(5)	1.36(15)	$E2$	7 203	$24^- \rightarrow 22^-$
1201.7	4(1)			11 442	$\rightarrow 30$
1209.3	314(16)	1.20(5)	$E2$	4 218	$18^+ \rightarrow 16^+$
1231.7	4(1)	0.46(12)	$M1$ or $E1$	10 355	$30 \rightarrow 29^-$
1251.9	5(1)			8 277	$\rightarrow 25^+$
1299.7	35(2)	1.21(6)	$E2$	8 325	$27^+ \rightarrow 25^+$
1349.5	6(1)			8 593	$27^- \rightarrow$
1381.2	2(1)			10 806	$\rightarrow 29^+$

[a]The uncertainties are between 0.2 and 1.0 keV depending on intensity.
[b]Intensities for γ rays are normalized to the 659.1 keV transition, with $I_\gamma = 1000$.
[c]Electric or magnetic nature of the transition has been determined by linear polarization measurement (see Fig. 1).
[d]Measurement of intensity or intensity ratio not possible due to presence of γ rays of overlapping energy.

respectively. In addition, several dipole transitions of energies 476.8, 351.0, 431.3, and 544.2 keV between bands 7 and 8 have been identified for the first time. An intense $E2$ transition of energy 427.1 keV has been observed from the 21^- level of band 10 to 19^- level of band 8. Linking transitions of energies 566.2, 312.2, 436.2, and 266.7 keV observed between bands 9 and 10 have also been placed.

A γ-ray transition of 419.8 keV energy from the 10^+ level of band 12 to the 9^- level of band 6 (see Fig. 2) was observed in the previous work [11]. In this work we could measure a positive Δ_{asym} value (see Fig. 1) and $R_\theta = 0.67$ for this transition which is consistent with its $E1$ character. With these results we could assign spins and parities to bands 11 and 12 unambiguously.

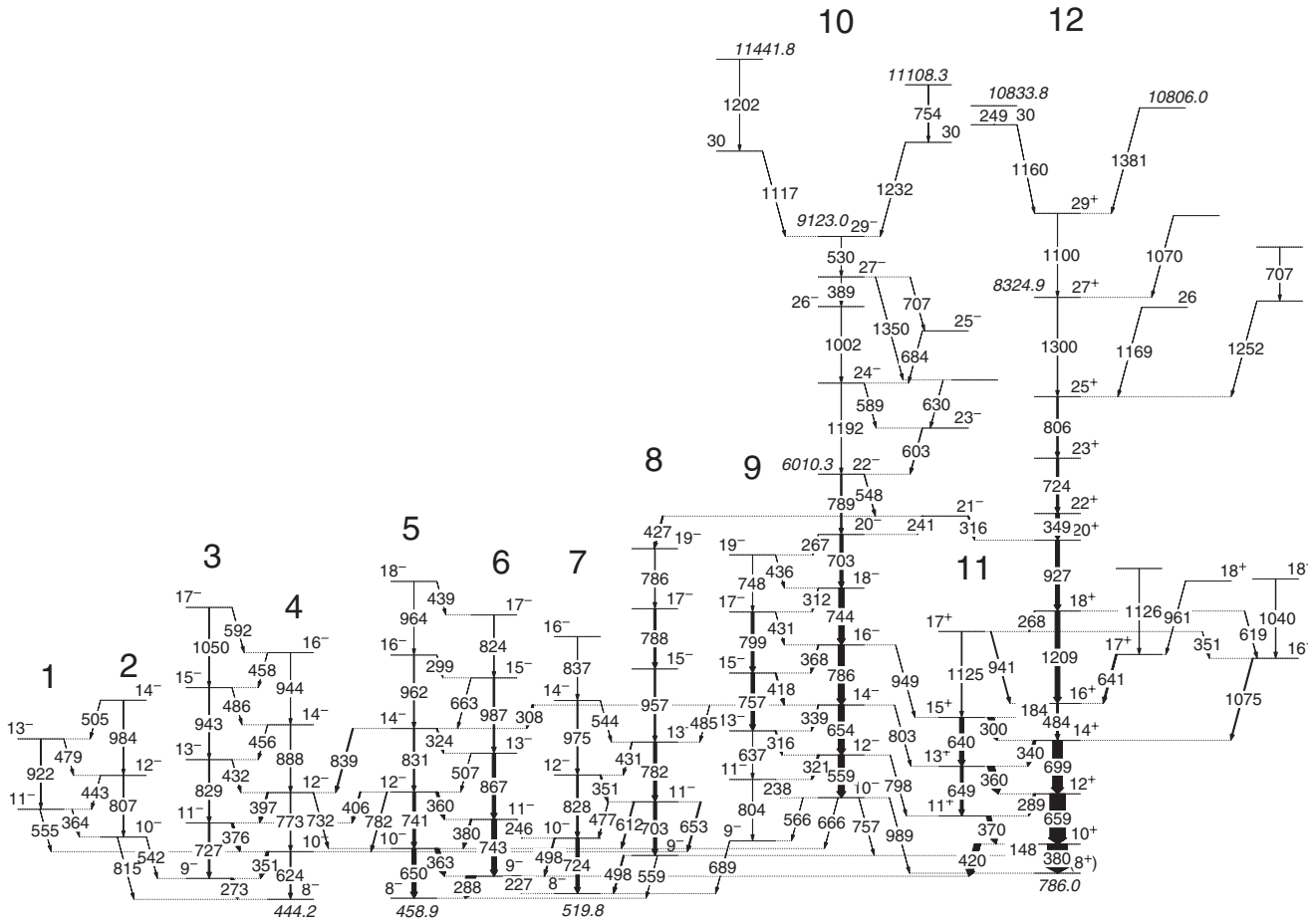

FIG. 2. Partial level scheme of ^{122}I.

B. Medium and high-spin results

Band 10 was reported in the earlier works by Moon *et al.* up to a tentative spin $I^{\pi} = (22^{-})$ [12,22], also see Ref. [19]. In this work we could extend this sequence up to a spin $I^{\pi} = 30^{-}$ and excitation energy 11 442 keV. In Fig. 3 a double-gated coincidence spectrum is displayed, where the newly observed transitions of band 10 can be seen. The γ rays of energies 1192.5, 1001.6, 388.7, and 529.9 keV have been observed in coincidence with the low-spin transitions of band 10. We have placed the cascade above the level at spin $I^{\pi} = 22^{-}$ of band 10. The observation of several crossover and decay out transitions from different levels further support their placement. The R_{θ} ratios for the 1192.5-, 1001.6-, and 529.9-keV transitions indicate their $E2$ nature (see Table I), while dipole nature could be revealed for the 388.7-keV γ ray. Hence, $I^{\pi} = 29^{-}$ has been assigned to the level at 9123 keV.

Above $I^{\pi} = 29^{-}$, the level scheme gets fragmented into two branches. One branch consists of two transitions of energy 1117.1 and 1201.7 keV and the other includes γ rays of energies 1231.7 and 753.6 keV. Figure 4 shows a double gated γ-ray coincidence spectrum, where the transitions feeding the state at $I^{\pi} = 29^{-}$ are visible. The angular distribution ratios for the 1117.1- and 1231.7-keV γ rays are compatible with $\Delta I = 1$ nature. The multipolarities of 1201.7 and 753.6 keV transitions could not be determined due to low statistics.

The positive parity states in band 12 were observed up to an excitation energy ~8.3 MeV [11]. However, multipolarities of high-spin transitions were uncertain. Present experiment extends the band further up to spin $I = 30$, and excitation energy 10 834 keV. Typical coincidence spectra for the high-spin regions are displayed in Figs. 5 and 6. The angular distribution ratios of the 805.9- and 1299.8-keV transitions are compatible with stretched $E2$ multipolarity, and thus, the level at 8325 keV is assigned a spin and parity of $I^{\pi} = 27^{+}$. A 1099.9 keV γ ray of $E2$ character has been placed above the 27^{+} level. The energy level at $I^{\pi} = 29^{+}$ is fed by two parallel γ-ray transitions of energies 1160.2 and 1381.2 keV. Moreover, a γ ray of energy 248.8 keV is observed in coincidence with 1160.2-keV transition. The angular distribution analysis confirms stretched dipole nature of the 1160.2-keV transition. The multipolarity of 1381.2- and 248.8-keV γ rays could not be determined.

IV. DISCUSSION

The ^{122}I nucleus was previously studied by Kaur *et al.* [21] and Moon *et al.* [12,22,23]. However, limited information is available on the configurations of band structures. In the following sections, configurations of the band structures in

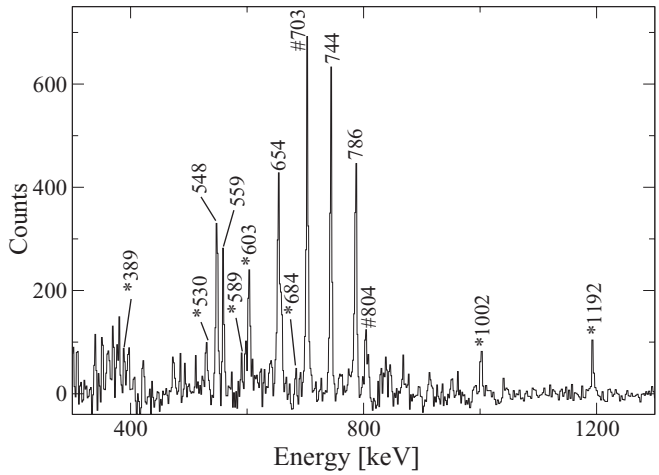

FIG. 3. Summed double gated γ-ray coincidence spectrum showing transitions of band 10. The spectrum was created with a gate on 241 keV transition and one from the list of 559-, 786-, 744-, 703-, and 548-keV γ rays. The peaks marked with asterisks denote transitions newly identified in the present work. Hash-marked peaks are unresolved doublets.

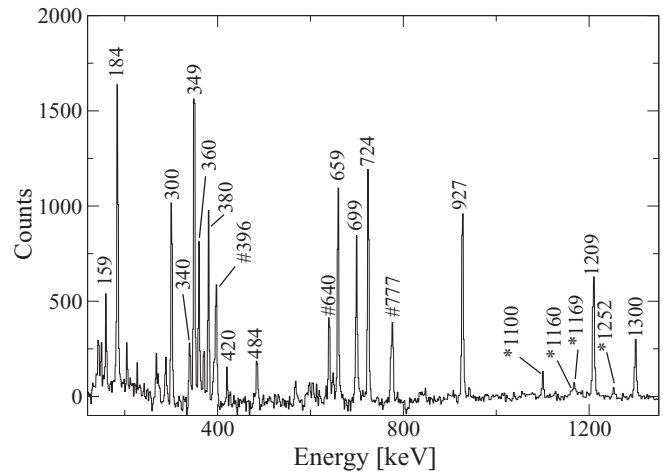

FIG. 5. Summed double gated γ-ray coincidence spectrum showing transitions of positive parity (band 12). The spectrum was created with a gate on 806-keV transition and one from a list of 659-, 699-, 300-, 184-, 1209-, 349-, and 724-keV γ rays. The peaks marked with asterisks denote transitions newly identified in the present work. Hash-marked peaks are unresolved doublets.

^{122}I will be discussed on the basis of observed band-crossing frequencies, corresponding alignment gains, as well as by comparing the experimental $B(M1)/B(E2)$ values with those predicted by the geometrical model of Dönau and Frauendorf [24,25]. The structure of high-spin states will be discussed within the framework of the CNS formalism.

A. Low- and medium-spin states

The $B(M1)/B(E2)$ ratios are extremely sensitive to the configuration involved and are very useful in assigning band configurations. Such ratios have been extracted for the strongly coupled bands in ^{122}I and are shown in Figs. 7 and 8. For this, spectra were produced by double gating on transitions above the level of interest and measuring the γ-ray branching ratio of the competing dipole ($\Delta I = 1$) and quadrupole ($\Delta I = 2$) transitions depopulating that level. Calculated $B(M1)/B(E2)$ ratios using the geometrical model of Dönau and Frauendorf [24,25] are also shown in Figs. 7 and 8. In these calculations, the $E2/M1$ mixing ratio for the dipole transitions is assumed to be small, and has been set to zero. The rotational gyromagnetic factor g_R has been taken as Z/A, and the relevant empirical g_k factors for the single particles have been adopted from [26]. The alignments i_x and the Ω values of the orbitals were

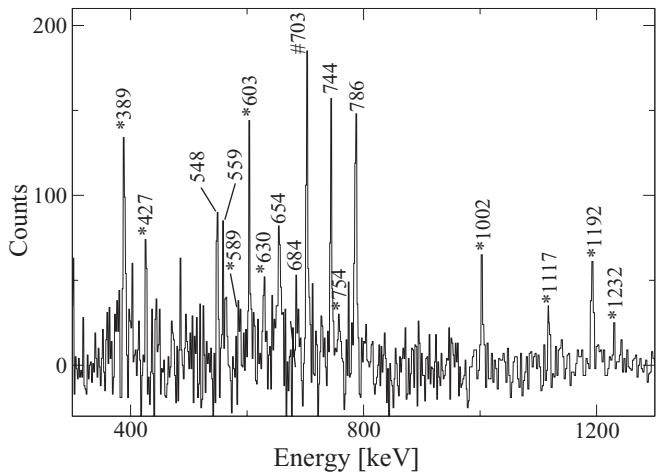

FIG. 4. Summed double gated γ-ray coincidence spectrum showing transitions feeding the state at $I^\pi = 29^-$ of band 10. The spectrum was created with a gate on 530-keV transition and one from the list of 559-, 786-, 744-, 703- and 548-keV γ rays. The peaks marked with hash are unresolved doublets. The peaks marked by asterisks are new transitions.

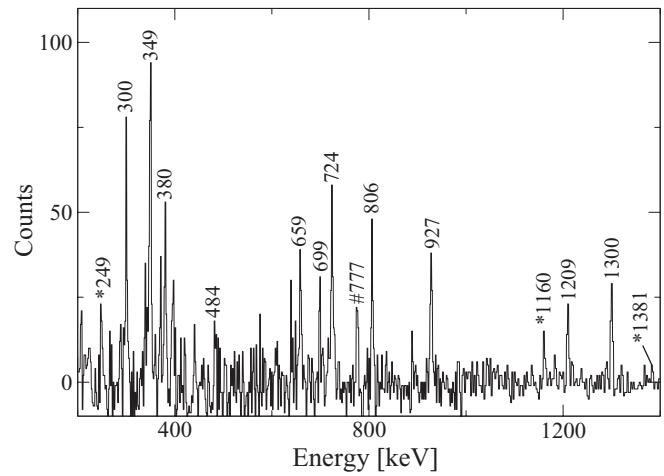

FIG. 6. Summed double gated γ-ray coincidence spectrum showing transitions of positive parity (band 12). The spectrum was created with a gate on 1100-keV transition and one from the list of all γ rays between 10^+ and 27^+ states of band 12, that is, between 659- and 1300-keV γ rays. The peaks marked with hash are unresolved doublets. The peaks marked by asterisks are new transitions.

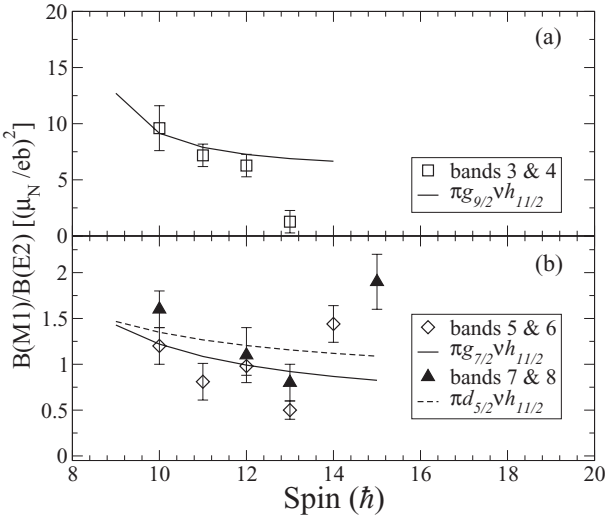

FIG. 7. $B(M1)/B(E2)$ ratios derived from γ-ray branching ratios for bands 3–8 in ^{122}I. The calculated values using the geometrical model of Dönau and Frauendorf for different configurations are shown as lines. Parameters used for the calculations of the predicted values : $i_p(g_{9/2}) = 0.5, i_p(g_{7/2}) = 2.5, i_p(d_{5/2}) = 1.5$, and $i_n(h_{11/2}) = 3.2$.

estimated from their Nilsson quantum numbers as well as systematics of bands based on similar structures in neighboring nuclei [27,28]. The value of quadrupole moment $Q_0 = 3.1e$ b has been taken from [8].

Strongly coupled bands built on $\Omega = 9/2([404]\frac{9^+}{2})$ orbital are one of the typical features in this mass region, and well established bands built upon above orbital are available in Sb, I, and light Cs nuclei. Most likely candidates for the $\pi g_{9/2}$ based bands in ^{122}I are the strongly coupled bands 1–4. The

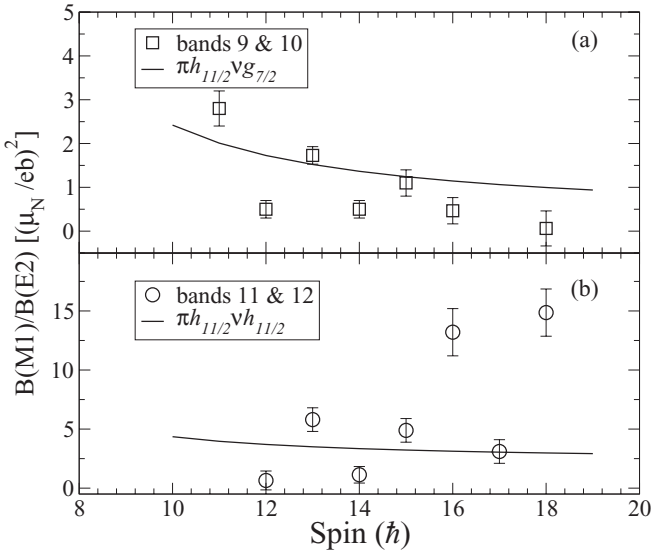

FIG. 8. $B(M1)/B(E2)$ ratios derived from γ-ray branching ratios for bands 9–12 in ^{122}I. The calculated values using the geometrical model of Dönau and Frauendorf for different configurations are shown as lines. Parameters used for the calculations of the predicted values : $i_p(h_{11/2}) = 5.0, i_n(g_{7/2}) = 0.5$, and $i_n(h_{11/2}) = 3.2$.

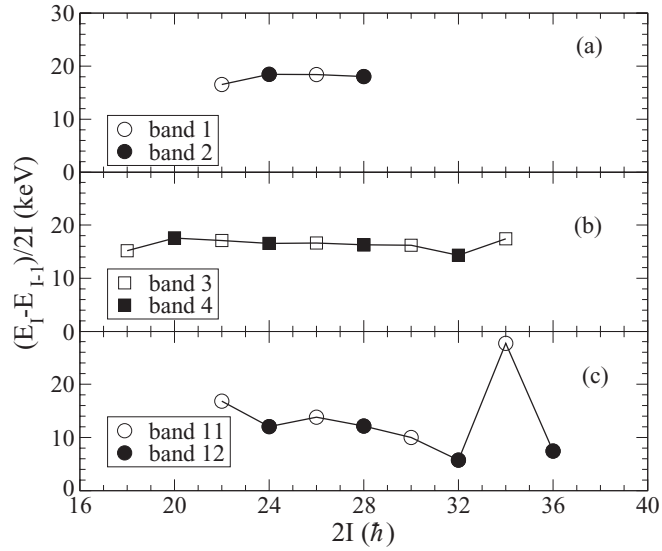

FIG. 9. $(E_I - E_{I-1})/2I$ plotted as a function of spin I (energy staggering plot) for bands 1–4 and bands 11 and 12.

lack of signature splitting, as shown in Fig. 9, is consistent with the above assignment. In previous work [21], bands 3 and 4 were assigned the $\pi g_{9/2} \otimes \nu h_{11/2}$ configuration. The experimental $B(M1)/B(E2)$ ratios for these bands are shown in Fig 7. They are compared to the ratio calculated using geometrical model for the $\pi g_{9/2} \otimes \nu h_{11/2}$ configuration. The reasonable agreement between experiment and theory supports the configuration proposed for these bands.

Bands 1 and 2 were weakly populated in the present experiment and it was not possible to extract electromagnetic properties of any of its transitions. The energy difference between states with same spin of bands 1 and 2, and those of bands 3 and 4 lies between 200 and 300 keV. Similar bands with energy difference between 300 and 400 keV have also been observed in neighboring iodine nuclei and have been interpreted in terms of coupling of $\pi g_{9/2}$ configuration with the γ vibration [8,29,30]. Therefore, a possible interpretation of bands 1 and 2 in ^{122}I is $\pi g_{9/2}\nu h_{11/2}$ configuration coupled to γ-phonon vibration.

Low-lying bands built on proton $d_{5/2}$ and $g_{7/2}$ orbitals have been established in all iodine nuclei. In the present work we have identified four $\Delta I = 2$ sequences, bands 5–8, which show characteristics similar to the $\pi g_{7/2} \otimes \nu h_{11/2}$ and $\pi d_{5/2} \otimes \nu h_{11/2}$ based bands in ^{126}Cs [31]. Presence of several $\Delta I = 1$ interlinking transitions observed between bands 5 and 6 and between bands 7 and 8 suggest that these bands are signature partners. The experimental aligned angular momenta i_x for the bands are plotted in Fig. 10. The Harris parameters $J_0 = 13\hbar^2/\text{MeV}$ and $J_1 = 35\hbar^4/\text{MeV}^3$ have been used to describe the energy of the rotating core. As shown in Fig. 10, bands 5–8 show up-bends at $\hbar\omega \sim 0.43$ MeV with gain in alignment $>4\hbar$. According to the cranked shell model calculations performed for nuclei in this mass region [21,28,32], the first and second $h_{11/2}$ neutron alignments occur at rotational frequencies $\hbar\omega \approx 0.35$ and $\hbar\omega \approx 0.45$, respectively. The blocking of first neutron crossing in all the above four bands (see Fig. 10) suggests that a neutron in $h_{11/2}$

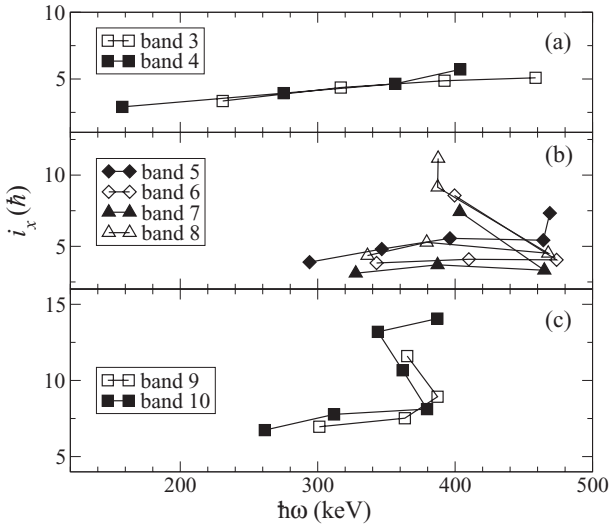

FIG. 10. Aligned angular momenta of (a) bands 3 and 4, (b) bands 5 and 6 and bands 7 and 8, and (c) bands 9 and 10. A reference core with Harris parameters $J_0 = 13\hbar^2$/MeV and $J_1 = 35\hbar^4$/MeV^3 was used.

is involved in their configurations. Furthermore, signature splitting in bands 7 and 8 is large compared to that of bands 5 and 6 (see Fig. 11). Therefore, configuration of bands 5 and 6 most likely involves a proton in $g_{7/2}$ ($\Omega = 3/2$), whereas a proton in the $d_{5/2}$ ($\Omega = 1/2$) orbital is responsible for bands 7 and 8. Therefore, we propose the $\pi g_{7/2} \otimes \nu h_{11/2}$ configuration for bands 5 and 6 and $\pi d_{5/2} \otimes \nu h_{11/2}$ configuration for bands 7 and 8. The calculated $B(M1)/B(E2)$ ratios for the assigned configurations, shown in Fig. 7, are also in reasonable agreement with those extracted experimentally for bands 5–8. One should note that the $d_{5/2}$ and $g_{7/2}$ orbitals mix strongly and the above configuration assignments are valid in the limit of low deformation.

Bands 9 and 10 show large initial alignment, $\sim 5\hbar$ (see Fig. 10), which suggests that the $h_{11/2}$ proton is involved in the configuration. However, no or small signature splitting supports involvement of high-Ω orbital, most likely $\Omega = 7/2$ of $\nu g_{7/2}$ orbital. Here, one should note that only the lower signature of $\pi h_{11/2}$ will contribute due to large signature splitting associated with $\Omega = 1/2$, whereas both the signatures of the $\nu g_{7/2}$ orbital will be involved in this configuration. The bands show an up-bend at frequencies about 0.36 MeV, which is attributed to the first pair of $h_{11/2}$ neutron alignment. The alignment gain of $\sim 6\hbar$ is consistent with the above aligning particles. Thus, we propose two-quasiparticle configuration, $\pi h_{11/2} \otimes \nu g_{7/2}$, below the band crossing and four-quasiparticle configuration, $\pi h_{11/2} \otimes [\nu g_{7/2}(\nu h_{11/2})^2]$, for the levels above the band crossings. The measured $B(M1)/B(E2)$ values are compared to the ratios calculated using the geometrical model in Fig. 8. Reasonable agreement has been observed for the above configuration. The $B(M1)/B(E2)$ ratios for the states above the band crossing could not be measured due to presence of γ-ray transitions of overlapping energies.

Positive parity bands 11 and 12 are the yrast sequences. In an earlier work by Kaur *et al.* [21], the $\pi(g_{7/2}/d_{5/2}) \otimes \nu h_{11/2}$ configuration was proposed for bands 11 and 12. Later, Moon *et al.* [11] suggested $\pi h_{11/2} \otimes \nu h_{11/2}$ configuration for the above bands. These bands show a much larger initial alignment ($\sim 7\hbar$) than any other bands of two-quasiparticle nature in ^{122}I. Such a large alignment can only be obtained by involving $h_{11/2}$ orbitals for both proton and neutron. In fact, bands with the above configuration have been observed in neighboring odd-odd Cs nuclei [28,31]. A nice agreement between experimental $B(M1)/B(E2)$ ratios and those calculated for the $\pi h_{11/2} \otimes \nu h_{11/2}$ configuration has been observed for lower spin states (see Fig. 8). An increase in the ratio observed above spin $I = 15$ may be due to noncollective nature of the states.

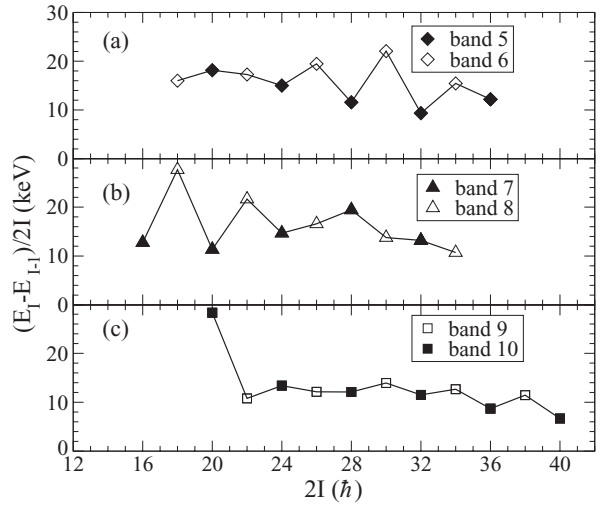

FIG. 11. $(E_I - E_{I-1})/2I$ plotted as a function of spin I (energy staggering plot) for bands 5–10.

B. High-spin behavior: Cranked Nilsson-Strutinsky calculations

In order to interpret high-spin states of ^{122}I, calculations were performed within the framework of the configuration-dependent cranked Nilsson-Strutinsky (CNS) formalism [33–35]. In this approach pairing is not included, which implies that the results are mainly relevant at high spin, where the effect of pairing is reduced. Within this approach, bands are formed for fixed configurations, specified by the number of particles in different $\mathcal{N}$-oscillator shells with signature $\alpha = +1/2$ and $\alpha = -1/2$, respectively. Furthermore, within the $\mathcal{N}$ shells, a distinction is made between the orbitals dominated by the highest-j shell and the other (low-j) shells, respectively. Within the fixed configurations, search for lowest-energy state at a given spin is made in a mesh of deformation space (ε_2, ε_4, γ), thus treating the collective and noncollective states on the same footing. For the parameters, κ and μ defining the $\vec{l} \cdot \vec{s}$ and l^2 strengths of the modified oscillator potential, the so-called $A = 110$ parameters were used [36]. These are known to give a good description of the smooth terminating bands in the neutron deficient $Z = 49$–54 nuclei [33]. The Lublin-Strasbourg drop (LSD) model [37] is used for the macroscopic energy, with the rigid-body moment of

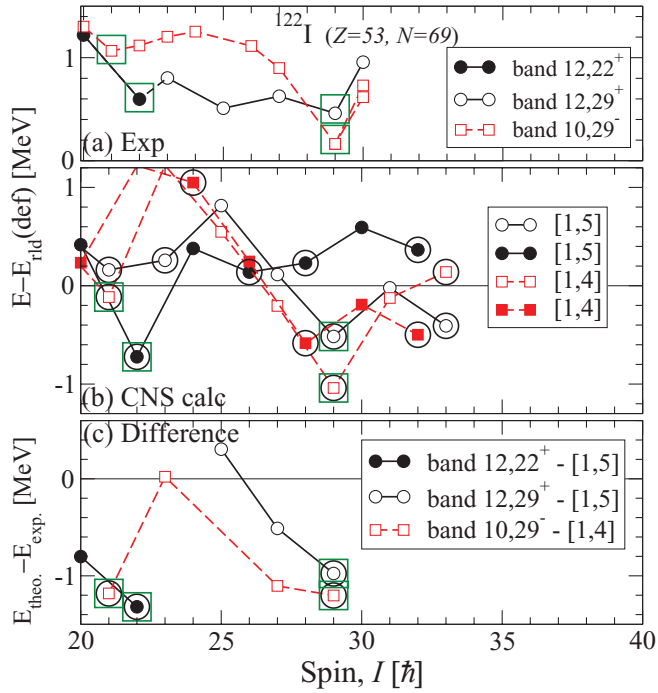

FIG. 12. (Color online) Energies, relative to a rotating-liquid-drop energy, for low-lying (a) observed and (b) calculated valence-space states for ^{122}I as well as (c) the difference between experiment and calculations. The calculated configurations are labeled by the number of $h_{11/2}$ protons and neutrons, respectively. Aligned states are encircled; open squares indicate the observed and corresponding calculated states, which appear especially low in energy.

inertia calculated with a radius parameter $r_0 = 1.16$ fm and a diffuseness parameter $a = 0.6$ fm [35].

In this calculation, the configurations are labeled relative to the ^{114}Sn core with a short-hand notation $[p_1,n_1]$, where p_1 and n_1 stand for number of protons and neutrons in $h_{11/2}$ orbitals, respectively. The remaining protons outside the core are distributed in orbitals of $g_{7/2}$ $d_{5/2}$ character, whereas neutrons are in $d_{3/2}$ and $s_{1/2}$ orbitals but with the possibility to make holes in the $d_{5/2}$ and $g_{7/2}$ orbitals if the $N = 64$ core is broken.

The excitation energy relative to a rotating liquid drop for the observed positive- and negative-parity states above spin $I = 20$ in ^{122}I is shown in the upper panel of Fig. 12. The low-lying high-spin states in the valence space are formed by coupling three protons outside the ^{114}Sn core as $\pi\{(d_{5/2}g_{7/2})^2_6(h_{11/2})^1_{11/2}\}_{23/2^-}$. This configuration is illustrated in a sloping Fermi surface diagram at a typical deformation $\varepsilon_2 = 0.15$ in the upper panel of Fig. 13. This proton configuration couples with the favored aligned neutron configurations $\nu\{(h_{11/2})^5_{35/2}(s_{1/2}d_{3/2})^0_0\}_{35/2^-}$ and $\nu\{(h_{11/2})^4_{16}(s_{1/2}d_{3/2})^1_{3/2}\}_{35/2^+}$ [see Fig. 13(b)] to obtain states with $I^\pi = 29^+$ and 29^-, respectively. The results obtained with the CNS calculations are shown in Fig. 12(b), where favored states are well reproduced. The difference between experiment and calculations is displayed in Fig. 12(c).

At somewhat lower spin, a favored state at $I^\pi = 21^-$ is observed in experiment as well as in CNS calculations for the

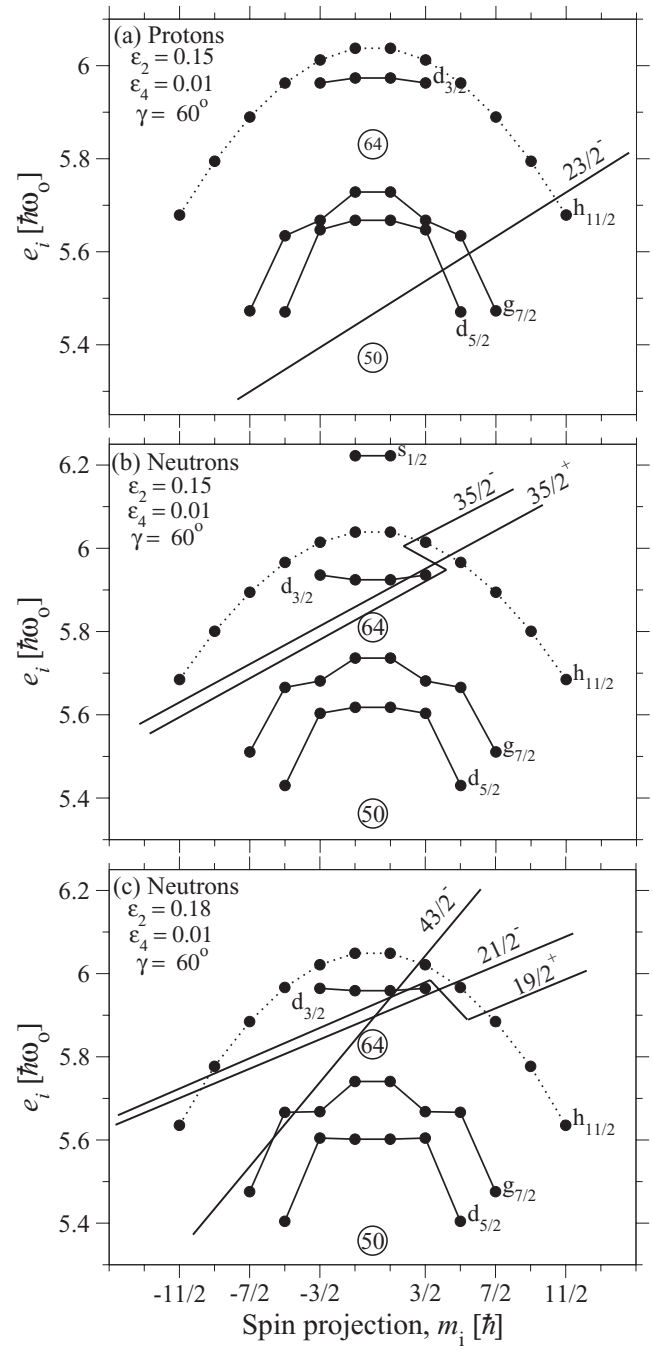

FIG. 13. The favored aligned states for (a) the $Z = 53$ configuration and $N = 69$ configurations with (b) all five neutrons aligned and with (c) one neutron antialigned. Configurations with four $h_{11/2}$ neutrons result in $I^\pi_n = 35/2^+$ and $19/2^+$ states, while five $h_{11/2}$ neutrons give $I^\pi_n = 35/2^-$ and $21/2^-$. The $43/2^-$ state is formed with five $h_{11/2}$ neutrons with one hole in the $N = 64$ core. The different structures are drawn close to their equilibrium deformations, which can be read from Figs. 14 and 15.

[1,4] configuration. The neutron configuration, as illustrated in lower panel of Fig. 13, can be understood as resulting from the transfer of one $h_{11/2}$ neutron from the $m_i = +5/2$ to the $m_i = -11/2$ orbital with respect to the fully aligned $I^\pi_n = 35/2^+$ state, shown in the middle panel.

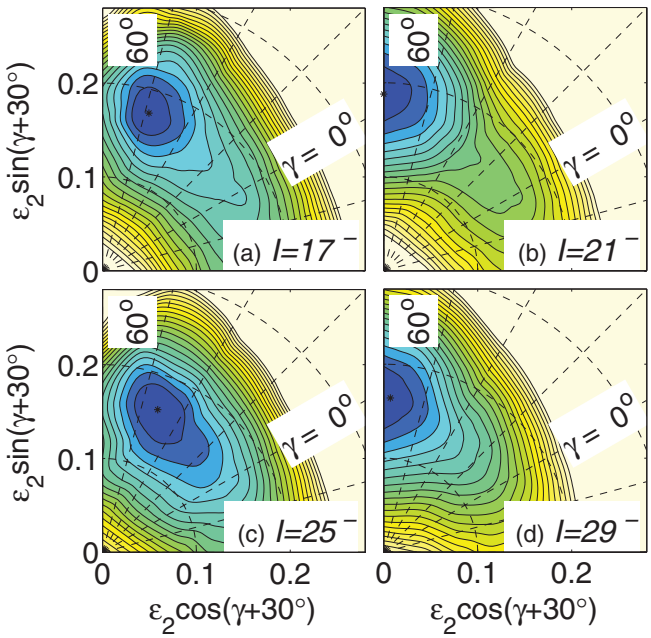

FIG. 14. (Color online) Calculated total energy surfaces for ^{122}I in the spin range $I^\pi = 17^-$–29^- of the $\pi h_{11/2}\nu(h_{11/2})^4$ configuration which is assigned to the observed negative-parity states (band 10). The contour line separation is 0.1 MeV.

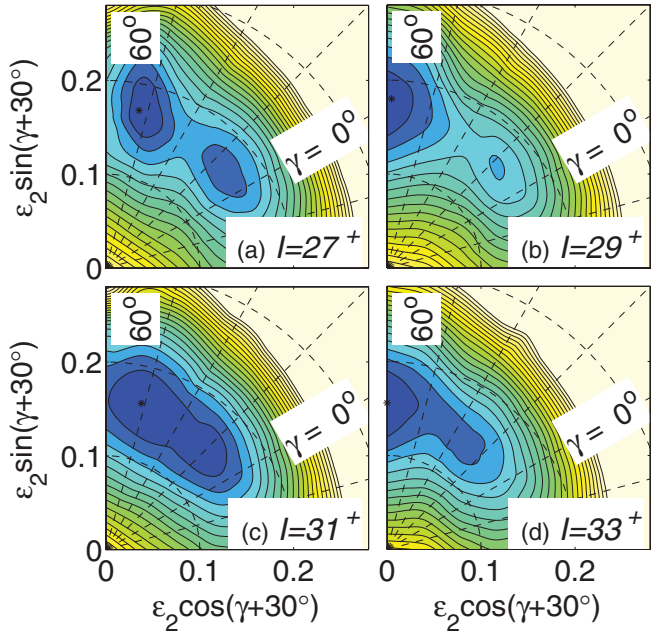

FIG. 15. (Color online) Calculated total energy surfaces for ^{122}I in the spin range $I^\pi = 27^+$–33^+ of the $\pi h_{11/2}\nu(h_{11/2})^5$ configuration which is assigned to the observed positive-parity states (band 12). The contour line separation is 0.1 MeV.

The calculated results for both signatures of the [1, 5] configuration are displayed in the middle panel of Fig. 12. It is evident from Fig. 12 that the $\alpha = 0$ states are less favored in energy at high spin and seem to have no experimental counter part. However, they appear at relatively lower energy at spin 22^+ with one spin vector antialigned at an approximate deformation $\varepsilon_2 = 0.18$ [see Fig. 13(c)] [38]. Therefore, we assign this configuration to the 22^+ state of band 12 in which a neutron is relocated from the $m_i = +3/2$ to the $m_i = -11/2$ orbital. The favored signature is assigned to high-spin states of band 12.

The differences in the lower panel of Fig. 12 are approximately constant at -1 MeV for the favored aligned and antialigned states. The fact that these differences are almost constant and lies within the same range as observed for terminating bands in this as well as other mass regions supports our interpretation of not only the fully aligned states but also of the states assigned as having one antialigned spin vector. For the other states in Fig. 12(c), the differences are more scattered, suggesting that they are difficult to describe with pure CNS configurations.

The potential energy surface (PES) plots for the configuration [1,4], assigned to the favored negative parity states, are shown in Fig. 14. At $I^\pi = 17^-$, a small collectivity is observed ($\gamma \approx 45°$). A noncollective minimum appears at $\gamma = 60°$ for $I^\pi = 21^-$, which is a state with one antialigned neutron, as discussed earlier. At higher spin, this minimum resurfaces at $\gamma \approx 40°$, and migrates toward lower collectivity with increasing spin and finally becomes oblate with $\gamma = 60°$ for $I^\pi = 29^-$ where the configuration terminates. The shift of the minimum in the PES calculations toward smaller ε_2 deformation with increasing spin is correlated with a decrease in the occupancy of high-Ω orbitals For example, both of the strongly deformation-driving $m_i = \pm 11/2$ states are occupied in the noncollective 21^- state, while only the $m_i = +11/2$ orbital is involved in the fully aligned 29^- state.

Several high-energy transitions feeding the maximally aligned states at $I^\pi = 29^-$ and $I^\pi = 29^+$ have been observed. Their excitation energies relative to a rotating liquid drop reference are displayed in Fig. 12(a). Although we could not assign parity to these states, it is still instructive to try to understand their configuration. The maximally aligned states in ^{122}I are generated by aligning the angular momenta of all the valence nucleons outside the ^{114}Sn core. Therefore, to generate higher angular momenta, neutrons from the orbitals of $g_{7/2}d_{5/2}$ character below the $N = 64$ shell gap have to be excited to the $d_{3/2}s_{1/2}$ or $h_{11/2}$ orbitals above the gap. For example, if we start with a neutron configuration with no holes in the $N = 64$ core and five $h_{11/2}$ particles [see Fig. 13(b)] then the next aligned state with a maximum neutron spin $I^\pi_n = 43/2^-$ and a total spin of $I^\pi = 33^+$ can be obtained by exciting one neutron from the $g_{7/2}d_{5/2}$ to $d_{3/2}s_{1/2}$ orbitals. This $I^\pi_n = 43/2^-$ state is illustrated in the Fig. 13(c). The PES plots for the [1, 5] configuration are shown in Fig. 15. At low spin ($I^\pi \leqslant 27^+$), a broad minimum is observed, consistent with a γ soft behavior. At $I^\pi = 29^+$ a favored noncollective minimum is observed corresponding to the maximally aligned state observed in experiment. The minimum at $I^\pi = 31^+$ shows small collectivity, most probably due to collective states formed by one neutron excitation from the $g_{7/2}d_{5/2}$ to $d_{3/2}s_{1/2}$ orbitals. This configuration terminates into a noncollective oblate state at $I^\pi = 33^+$. A less favored minimum appearing at these spins (at $\gamma \sim 15°$) corresponds to a configuration

involving a two neutron excitation from the $g_{7/2}d_{5/2}$ to $d_{3/2}s_{1/2}$ orbitals. This configuration will terminate at $I^{\pi} = 37^{+}$.

Another reasonable interpretation for these states can be understood from Fig. 12(b), where the two signatures of the [1,4] configuration are drawn up to higher spin. Again, the corresponding states having negative parity are created by exciting neutrons from the $g_{7/2}d_{5/2}$ orbitals to $d_{3/2}s_{1/2}$. There is a favorable aligned state at spin $I^{\pi} = 32^{-}$ with $\alpha = 0$ signature, whereas the aligned state in other signature is unfavored. Further possibilities may involve states with six $h_{11/2}$ neutrons and with hole(s) in the $N = 64$ core.

V. SUMMARY

In summary, excited states of ^{122}I were populated via the ^{116}Cd(^{11}B,5n)^{122}I reaction at a beam energy of 65 MeV. The level scheme of ^{122}I has been extended up to an excitation energy of 11.5 MeV and spin $\sim 30\hbar$. Configurations of the bands have been discussed using the alignments, band crossing frequencies, and electromagnetic properties. At high spin, specific states have been identified in experiment with calculated maximal spin aligned states built on the valence space configurations $\nu[(h_{11/2})^5]$ and $\nu[(h_{11/2})^4(s_{1/2}d_{3/2})^1]$ combined with the $\pi[h_{11/2}(g_{7/2}d_{5/2})^2]$ configuration. In addition, favored noncollective states where one particle is antialigned have also been identified at $I^{\pi} = 21^{-}$ and 22^{+}. Structures above the maximally aligned states at $I^{\pi} = 29^{+}$ and 29^{-} have been identified in the CNS calculation as one or two neutron excitation across the $N = 64$ shell gap.

ACKNOWLEDGMENTS

The authors thank the staff at TIFR-BARC pelletron accelerator and target laboratory staff of VECC for their excellent support. P.S. [Contract No. 9/81(1108)/10-EMR-I] and S.N. [Contract No. 09/081(0704)/2009- EMR-I] acknowledge financial support from CSIR India. This work was supported by the DST India and the Swedish Science Research Council.

[1] E. S. Paul *et al.*, J. Phys. G **18**, 837 (1992).
[2] M. P. Waring, D. B. Fossan, J. R. Hughes, D. R. LaFosse, Y. Liang, R. Ma, P. Vaska, E. S. Paul, S. A. Forbes, R. Wadsworth, and R. M. Clark, Phys. Rev. C **48**, 2629 (1993).
[3] Y. Liang *et al.*, Phys. Rev. C **45**, 1041 (1992).
[4] Y. Liang *et al.*, Phys. Rev. C **44**, R578 (1991).
[5] P. Singh *et al.*, Phys. Rev. C **85**, 034319 (2012).
[6] P. Singh *et al.*, Phys. Rev. C **82**, 034301 (2010).
[7] E. S. Paul *et al.*, Phys. Rev. C **45**, R2531 (1992).
[8] S. Törmänen *et al.*, Nucl. Phys. A **613**, 282 (1997).
[9] E. S. Paul *et al.*, Phys. Rev. C **59**, 1984 (1999).
[10] E. S. Paul *et al.*, J. Phys. G **19**, 913 (1993).
[11] C.-B. Moon, G. D. Dracoulis, R. A. Bark, A. P. Byrne, P. A. Davidson, A. N. Wilson, A. M. Baxter, T. Kibedi, and G. J. Lane, J. Korean Phys. Soc. **43**, S100 (2003).
[12] C. B. Moon, G. D. Dracoulis, R. A. Bark, A. P. Byrne, P. M. Davidson, A. N. Wilson, T. Kibedi, G. J. Lane, and A. M. Baxter, Australian National Univ., Dept. of Nuclear Physics 2002 Annu. Rep., p. 13 (2003); ANU-P/1564 (2003).
[13] R. Palit *et al.*, Nucl. Instrum. Methods A **680**, 90 (2012).
[14] R. Palit, AIP Conf. Proc. **1336**, 573 (2011).
[15] D. C. Radford, Nucl. Instrum. Methods A **361**, 297 (1995).
[16] R. E. Shroy, D. M. Gordon, M. Gai, D. B. Fossan, and A. K. Gaigalas, Phys. Rev. C **26**, 1089 (1982).
[17] G. Duchêne *et al.*, Nucl. Instrum. Methods Phys. Res. Sect. A **432**, 90 (1999).
[18] K. Starosta *et al.*, Nucl. Instrum. Methods Phys. Res. Sect. A **423**, 16 (1999).
[19] T. Tamura, Nucl. Data Sheets **108**, 455 (2007).
[20] M. A. Quader, W. F. Piel, Jr., S. Vajda, W. A. Watson III, F. C. Yang, and D. B. Fossan, Phys. Rev. C **30**, 1772 (1984).
[21] H. Kaur, J. Singh, A. Sharma, D. Mehta, N. Singh, P. N. Trehan, H. C. Jain, S. D. Paul, E. S. Paul, and R. K. Bhowmik, Phys. Rev. C **55**, 2234 (1997).
[22] C.-B. Moon, G. D. Dracoulis, R. A. Bark, A. P. Byrne, P. A. Davidson, T. Kibedi, G. J. Lane, and A. N. Wilson, J. Korean Phys. Soc. **59**, 1525 (2011).
[23] C. B. Moon, J. Korean Phys. Soc. **44**, 244 (2004).
[24] F. Dönau, Nucl. Phys. A **471**, 469 (1987).
[25] S. Frauendorf, Phys. Lett. B **100**, 219 (1981).
[26] T. Lönnroth, S. Vajda, O. C. Kistnerand, and M. H. Rafailovich, Z. Phys. A **317**, 215 (1984).
[27] D. Ward *et al.*, Nucl. Phys. A **529**, 315 (1991).
[28] A. Gizon *et al.*, Nucl. Phys. A **694**, 63 (2001).
[29] C.-B. Moon, T. Komatsubara, T. Shizuma, Y. Sasaki, H. Ishiyama, T. Jumatsu, and K. Furuno, Eur. Phys. J. A **5**, 13 (1999).
[30] C.-B. Moon *et al.*, J. Korean Phys. Soc. **53**, 1844 (2008).
[31] S. Wang, Y. Liu, Y. Ma, T. Komatsubara, and Y. Zhang, Phys. Rev. C **75**, 037302 (2007).
[32] H. Kaur, J. Singh, A. Sharma, J. Goswamy, D. Mehta, N. Singh, P. N. Trehan, E. S. Paul, and R. K. Bhowmik, Phys. Rev. C **55**, 512 (1997).
[33] A. V. Afanasjev, D. B. Fossan, G. J. Lane, and I. Ragnarsson, Phys. Rep. **322**, 1 (1999).
[34] T. Bengtsson and I. Ragnarsson, Nucl. Phys. A **436**, 14 (1985).
[35] B. G. Carlsson and I. Ragnarsson, Phys. Rev. C **74**, 011302(R) (2006).
[36] Jing-ye Zhang, N. Xu, D. B. Fossan, Y. Liang, R. Ma, and E. S. Paul, Phys. Rev. C **39**, 714 (1989).
[37] K. Pomorski and J. Dudek, Phys. Rev. C **67**, 044316 (2003).
[38] I. Ragnarsson and T. Bengtsson, Nucl. Phys. A **447**, 251c (1985).